Research Square

Preprints are preliminary reports that have not undergone peer review.
They should not be considered conclusive, used to inform clinical practice,
or referenced by the media as validated information.

A Jacobsthal Window in Exoplanet Period Ratios: Derivation of the 71/35 Offset from Symplectic Depletion

David Coates

coates.research@protonmail.com

Independent researcher

Research Article

Keywords: exoplanets, celestial mechanics, orbital resonance, symplectic maps, dynamical systems

Posted Date: March 23rd, 2026

DOI: https://doi.org/10.21203/rs.3.rs-9174328/v1

License: This work is licensed under a Creative Commons Attribution 4.0 International License.
Read Full License

Additional Declarations: The authors declare no competing interests.

A Jacobsthal Window in Exoplanet Period Ratios: Derivation of the 71/35 Offset from Symplectic Depletion

D. Coates
Independent Researcher, Belfast, Northern Ireland
coates.research@protonmail.com

Draft version March 20, 2026

Abstract

The distribution of period ratios in multi-planet systems shows a systematic displacement from the exact 2:1 mean-motion resonance. Using 1038 confirmed multi-planet systems from the NASA Exoplanet Archive (1555 adjacent pairs), we identify 56 pairs within the interval [2.000, 43/21] and measure their mean period ratio as $\langle R\rangle = 2.027 \pm 0.004$ (bootstrap 95% CI), significantly above exact commensurability ($p < 10^{-5}$, Wilcoxon) and statistically consistent with our predicted value ($p = 0.67$, Wilcoxon).

We derive a quantitative model for this offset. The symplectic transfer matrix $T(k)$ governs near-resonant dynamics; at the stability boundary $k = 2$, it generates the Hamiltonian Möbius map $g(r) = 2 - 1/r$, which drives ratios away from 2. We show that adding the unique linear state-dependent dissipation $\gamma(r) = 3 - r$—stronger near resonance, vanishing far from it—converts g exactly into the Jacobsthal map $f(r) = 1 + 2/r$, whose iterates are the Jacobsthal ratios $J(n+1)/J(n)$ converging to 2.

The deviation identity $J(n+1)/J(n) - 2 = (-1)^n/J(n)$ places the dominant low-order attractor above 2:1 at $43/21 = 2 + 1/21$, defining a resonance window of width $\Delta = 1/21$. Spectral-edge depletion near the boundary distributes systems within this window as $\rho(x) \propto \sqrt{x}$, yielding

$$\langle R\rangle - 2 \;=\; \tfrac{3}{5}\,\Delta \;=\; \tfrac{1}{35} \;\approx\; 0.02857,$$

predicting $\langle R\rangle = 71/35 \approx 2.0286$. A KS test on the wider interval [1.95, 2.10] gives $p = 0.80$.

Four independent lines of evidence support the framework: (i) REBOUND N-body migration simulations cluster at $43/21 = 2.048$, not 2.000; (ii) TRAPPIST-1 non-adjacent period ratios align with Jacobsthal values (permutation $p = 0.0004$); (iii) the Beta Pictoris system architecture at 30–36 AU matches the Jacobsthal framework, independently confirmed at 30–35 AU; (iv) Monte Carlo experiments confirm the $\sqrt{\epsilon}$ edge exponent under migration-weighted ensembles. The model has no free parameters.

exoplanets — celestial mechanics — orbital resonance — symplectic maps — dynamical systems

1 Introduction

The period-ratio distribution of adjacent planet pairs exhibits prominent features near low-order mean-motion resonances, especially 3:2 and 2:1 (Fabrycky et al., 2014; Steffen & Hwang, 2015; Lissauer et al., 2011; Winn & Fabrycky, 2015). A persistent observation is that systems near 2:1 are displaced to slightly larger values rather than accumulating at exact commensurability (Fabrycky et al., 2014; Lithwick & Wu, 2012).

Existing explanations invoke dissipative migration, resonant repulsion, or post-disk evolution (Lithwick & Wu, 2012; Batygin & Morbidelli, 2013; Deck & Batygin, 2015; Chatterjee & Ford, 2015). These mechanisms are well motivated but do not predict a preferred numerical offset. The question addressed here is: can the magnitude of the offset be derived from the structure of the stability boundary?

We show that it can. The predicted mean period ratio is $\langle R\rangle = 71/35 \approx 2.029$, with no free parameters. The observed value is 2.027 ± 0.004.

The model has three elements:

1. A dynamical derivation showing that the Hamiltonian map at the stability boundary, combined with state-dependent dissipation, produces the Jacobsthal map exactly (Section 2);

2. The Jacobsthal deviation identity, identifying the dominant low-order attractor above 2:1 (Section 3);

3. Spectral-edge depletion near $|\mathrm{Tr}(M)| = 2$, distributing systems within the resulting resonance window (Section 4).

Together these yield $\langle R \rangle = 71/35$ with no free parameters. Four independent empirical tests support the framework (Sections 5–8).

2 Dynamical Origin of the Jacobsthal Attractor

2.1 The Transfer Matrix and the Stability Boundary

Near a mean-motion resonance, the local dynamics of a weakly perturbed planetary pair can be described by an area-preserving map whose linear stability is governed by a transfer matrix $M \in \mathrm{SL}(2, \mathbb{R})$ (Meiss, 1992; Wisdom, 1980, 1983; Henrard & Lemaître, 1983). In the standard normal form, this takes the one-parameter family

$$T(k) = \begin{pmatrix} k & -1 \\ 1 & 0 \end{pmatrix}, \quad \det T(k) = 1, \tag{1}$$

where $k = \mathrm{Tr}(M)$. The eigenvalues are $\lambda_\pm = (k \pm \sqrt{k^2 - 4})/2$. For $|k| < 2$ they are complex conjugate on the unit circle (stable); for $|k| > 2$ they are real and reciprocal (unstable). The boundary $|k| = 2$ is the parabolic transition.

2.2 The Conservative Map at the Boundary

The transfer matrix (1) acts on the ratio $r_n = x_{n+1}/x_n$ of consecutive iterates via the Möbius map

$$g_k(r) = k - \frac{1}{r}. \tag{2}$$

At the stability boundary $k = 2$, this becomes

$$g(r) = 2 - \frac{1}{r}, \tag{3}$$

whose fixed point satisfies $r^2 - 2r + 1 = (r-1)^2 = 0$, giving $r^* = 1$ (degenerate). Starting from $r = 2$, the iterates of g are

$$2,\ \frac{3}{2},\ \frac{4}{3},\ \frac{5}{4},\ \frac{6}{5},\ \ldots\ \to\ 1. \tag{4}$$

This is the Hamiltonian dynamics at the boundary: ratios decay monotonically from 2 toward the degenerate eigenvalue $r^* = 1$. The Jordan-block structure of $T(2)$ drives the system away from the boundary value. Conservative dynamics alone cannot explain accumulation near $R = 2$.

2.3 Dissipation Converts the Hamiltonian Map into the Jacobsthal Map

In a dissipative system (e.g., a planet pair migrating through a gas disk), the transfer matrix is no longer area-preserving: $\det M < 1$. The simplest parameterisation introduces a damping factor $\gamma \in [0, 1]$ that reduces the memory term in the Möbius map:

$$g_\gamma(r) = 2 - \frac{1-\gamma}{r}. \tag{5}$$

At $\gamma = 0$ this is the conservative map $g(r)$; at $\gamma = 1$ it reduces to the constant 2 (total dissipation).

If the damping rate depends on the distance from resonance—stronger dissipation for systems closer to exact commensurability, weaker for systems far from it—then γ becomes a function of r. We ask: what dissipation $\gamma(r)$ converts the Hamiltonian map into a map whose fixed point is the boundary value $r^* = 2$?

Setting $g_\gamma(r) = f(r) \equiv 1 + 2/r$ and solving for γ:

$$2 - \frac{1-\gamma}{r} = 1 + \frac{2}{r} \implies 1 - \gamma = \frac{r-2}{1} \implies \gamma(r) = 3 - r. \tag{6}$$

Theorem 1 (Dissipative Selection of the Jacobsthal Map). *The unique linear state-dependent dissipation $\gamma(r) = 3 - r$ converts the Hamiltonian boundary map $g(r) = 2 - 1/r$ into the Jacobsthal map $f(r) = 1 + 2/r$ exactly.*

Proof. Substituting $\gamma = 3 - r$ into (5):

$$g_\gamma(r) = 2 - \frac{1-(3-r)}{r} = 2 - \frac{r-2}{r} = 2 - 1 + \frac{2}{r} = 1 + \frac{2}{r} = f(r).$$

The dissipation $\gamma(r) = 3 - r$ has physically correct properties:

- At exact resonance $r = 2$: $\gamma = 1$ (maximum dissipation).
- At the Jacobsthal attractor $r = 43/21 \approx 2.048$: $\gamma = 20/21 \approx 0.95$ (strong).
- At $r = 3$ (the first Jacobsthal iterate, far from resonance): $\gamma = 0$ (no dissipation—the system is conservative).
- The physical range $\gamma \in [0, 1]$ corresponds to $r \in [2, 3]$, which covers the resonance zone.

The value $\gamma(2) = 1$ is a formal endpoint of the map, not a claim that real systems experience instantaneous locking at exact commensurability. The spectral-edge depletion (Section 4) ensures that effectively no systems reach $r = 2$; the dynamics are governed by γ evaluated over the Jacobsthal window

$r \in [2,\ 43/21]$, where $\gamma \in [0.95,\ 1]$ and the distinction between total and near-total dissipation is immaterial.

The effective determinant of the dissipative map is $\det M_\gamma = 1 - \gamma = r - 2$. At the dominant attractor $r = 43/21$:

$$\det M_\gamma = \frac{43}{21} - 2 = \frac{1}{21} = \Delta, \tag{7}$$

where Δ is the Jacobsthal window width. The map's area contraction at the dominant attractor is the window width—a relationship that connects the dissipation physics directly to the resonance-window structure.

This derivation resolves the central theoretical question: the Jacobsthal map $f(r)$ is not introduced as an independent ansatz but arises from the Hamiltonian map $g(r)$ at the stability boundary when state-dependent dissipation $\gamma(r) = 3 - r$ is included. The dissipation profile—stronger near resonance, vanishing far from it—is the generic behavior of both tidal and disk-driven migration.

2.4 The Jacobsthal Iterates (Proof)

The fixed points of $f(r) = 1 + 2/r$ satisfy $r^2 - r - 2 = (r-2)(r+1) = 0$, giving $r^* = 2$ (stable, attracting) and $r^* = -1$ (unstable). Starting from $r = 1$, the iterates are the Jacobsthal ratios:

$$1,\ 3,\ \frac{5}{3},\ \frac{11}{5},\ \frac{21}{11},\ \frac{43}{21},\ \frac{85}{43},\ \ldots\ \to\ 2, \tag{8}$$

oscillating around $r^* = 2$ with alternating overshoots and undershoots.

Theorem 2 (Jacobsthal Iterates). *The iterates of $f(x) = 1 + 2/x$ starting from $x_0 = 1$ are exactly the Jacobsthal ratios:*

$$x_n = \frac{J(n+2)}{J(n+1)}, \quad n = 0, 1, 2, \ldots \tag{9}$$

where $J(n) = J(n-1) + 2\,J(n-2)$ with $J(0) = 0$, $J(1) = 1$.

Proof. By induction. The base case $x_0 = 1 = J(2)/J(1)$ holds. For the inductive step, if $x_n = J(n+2)/J(n+1)$, then

$$x_{n+1} = 1 + \frac{2}{x_n} = 1 + \frac{2\,J(n+1)}{J(n+2)} = \frac{J(n+2) + 2\,J(n+1)}{J(n+2)} = \frac{J(n+3)}{J(n+2)},$$

where the last step uses the Jacobsthal recurrence.

2.5 Connection to Period Ratio

For a near-resonant pair with nominal resonance $p\!:\!q$, the trace $k = \mathrm{Tr}(M)$ of the monodromy matrix is a smooth function of the period ratio R and the orbital eccentricities, with $k = 2$ at exact commensurability $R = p/q$ (Henrard & Lemaître, 1983; Murray & Dermott, 1999). Expanding near the boundary:

$$k(R) \approx 2 + \alpha\,(R-2) + \beta\,(R-2)^2 + \mathcal{O}(R-2)^3, \tag{10}$$

where the coefficients depend on mass ratio μ and eccentricity. For the super-Earth population dominating the Kepler sample ($\mu \sim 10^{-5}$, $e \sim 0.01$), expansion of the pendulum Hamiltonian near resonance (Henrard & Lemaître, 1983) gives $\alpha \approx 1.2$ and $\beta \approx -0.8$. Across the Jacobsthal window ($\Delta = 1/21 \approx 0.048$), the quadratic term contributes $|\beta|\,\Delta^2 \approx 0.002$ to k, which is 30 times smaller than the linear variation $\alpha\,\Delta \approx 0.058$. The linear approximation thus introduces error < 0.001 in the predicted period ratio—negligible compared to the observational uncertainty (± 0.004).

For more massive planets ($\mu \sim 10^{-3}$), the resonance half-width $\mu^{2/3} \sim 0.01$ becomes comparable to $\Delta/2$, and the sharp-window approximation may break down.

2.6 Physical Grounding of the Dissipation Profile

The profile $\gamma(r) = 3 - r$ was derived in Section 2.3 as the unique linear function converting the Hamiltonian map into the Jacobsthal map. We now show that this profile is the leading-order approximation to any physically motivated resonant coupling, with quantifiable error.

The boundary conditions are not independent. At $r = 3$, the conservative and Jacobsthal maps coincide exactly:

$$g(3) = 2 - \tfrac{1}{3} = \tfrac{5}{3} = 1 + \tfrac{2}{3} = f(3), \tag{11}$$

so any dissipation that converts g into f *must* vanish at $r = 3$. This is not imposed—it is a self-consistency condition. The point $r = 3$ corresponds to the adjacent 3:1 mean-motion resonance, where the 2:1 disturbing function loses dynamical control (Chirikov, 1979). The physical picture is therefore: the effective dissipation saturates at exact commensurability ($\gamma = 1$ at $r = 2$) and vanishes at the Chirikov boundary of the 2:1 resonance zone ($\gamma = 0$ at $r = 3$).

Any smooth, monotonically decreasing coupling $\gamma(r)$ satisfying these two boundary conditions has the

Taylor expansion

$$\gamma(r) = 1-(r-2)+\mathcal{O}\big((r-2)^2\big) = 3-r+\mathcal{O}\big((r-2)^2\big). \tag{12}$$

Over the Jacobsthal window ($\Delta = 1/21 \approx 0.048$), the quadratic remainder contributes $|\kappa|\,\Delta^2$ to γ, where κ is the curvature of the physical coupling.

To estimate κ, we compute the normalized resonant coupling from the Laplace coefficient of the 2:1 disturbing function. The leading term is $C(r) = \alpha\, b^{(2)}_{1/2}(\alpha)$, where $\alpha = r^{-2/3}$ (Kepler's third law) and $b^{(j)}_s$ is the standard Laplace coefficient (Murray & Dermott, 1999). Normalizing so that $\gamma_{\rm Lap}(2) = 1$ and $\gamma_{\rm Lap}(3) = 0$ and fitting a quadratic gives curvature $\kappa \approx 0.66$. Over the Jacobsthal window, this yields:

$$|\kappa|\,\Delta^2 \approx 0.0015, \tag{13}$$

which shifts the predicted $\langle R\rangle$ by $\frac{3}{5}\,|\kappa|\,\Delta^2 \approx 0.0009$—less than one-quarter of the observational uncertainty (± 0.004). The prediction $\langle R\rangle = 71/35$ is therefore robust to the nonlinearity of the physical coupling.

An alternative estimate using the resonance-width scaling $\gamma_{\rm w}(r) \propto |C(r)|^{2/3}$ (proportional to the libration half-width in the pendulum approximation) gives even closer agreement: the maximum deviation from $\gamma = 3-r$ over the Jacobsthal window is 0.013, corresponding to a shift in $\langle R\rangle$ of < 0.0004.

In summary, the dissipation profile $\gamma(r) = 3-r$ is not an *ad hoc* choice. It is the leading approximation to any resonant coupling bounded by exact commensurability and the adjacent resonance zone, with corrections that are negligible over the narrow Jacobsthal window. Hydrodynamic verification of the profile shape remains a worthwhile target for future work, but the current prediction does not depend on it.

3 The Jacobsthal Deviation Identity

The Jacobsthal sequence has closed form $J(n) = (2^n - (-1)^n)/3$. The deviation of consecutive ratios from the limiting value obeys:

$$\frac{J(n+1)}{J(n)} - 2 = \frac{(-1)^n}{J(n)}. \tag{14}$$

Proof. From $J(n+1) = J(n) + 2\,J(n-1)$:

$$\frac{J(n+1)}{J(n)} - 2 = \frac{2\,J(n-1) - J(n)}{J(n)}. \tag{15}$$

Using the closed form:

$$2\,J(n-1) - J(n) = \frac{2(2^{n-1} - (-1)^{n-1}) - (2^n - (-1)^n)}{3} = \frac{(-1)^n \cdot 3}{3} = \tag{16}$$

3.1 Even-Index Parity Structure

At even indices, the Jacobsthal sequence satisfies the affine relation

$$J(2k+1) = 2\,J(2k) + 1, \tag{17}$$

giving $J(2k+1)/J(2k) = 2 + 1/J(2k) > 2$. At odd indices, $J(2k+2) = 2\,J(2k+1) - 1$, giving ratios below 2. The even-index branch produces all above-boundary convergents.

The dominant (lowest-order) even-index ratio is

$$\frac{J(7)}{J(6)} = \frac{43}{21} = 2 + \frac{1}{21} \approx 2.048. \tag{18}$$

In the KAM hierarchy (Wisdom, 1980; Chirikov, 1979), low-denominator resonances are the most dynamically significant.

4 The Jacobsthal Window and Wigner Integral

The interval between exact 2:1 and the dominant above-boundary convergent defines the Jacobsthal window:

$$\Delta = \frac{43}{21} - 2 = \frac{1}{21}. \tag{19}$$

The attractor 43/21 acts as a dynamical barrier: systems migrating inward encounter this convergent before reaching exact 2:1. Those that are not captured at 43/21 continue toward the boundary, but the spectral-edge depletion progressively thins their ranks. The $\sqrt{x}$ density describes the distribution of systems that have passed the attractor and are approaching—but cannot reach—exact commensurability. The density is lowest near $x = 0$ (the boundary) and highest near $x = \Delta$ (the attractor), consistent with the histogram in Figure 1(b).

The spectral density of $\mathrm{SL}(2,\mathbb{R})$ matrices under the Haar measure vanishes as $\sqrt{\epsilon}$ at the boundary $k = 2$ (Mehta, 2004):

$$\rho(k) = \frac{1}{2\pi}\sqrt{4-k^2} \;\xrightarrow{k\to 2^-}\; \frac{1}{\pi}\,\sqrt{\epsilon}, \tag{20}$$

where $\epsilon = 2-k$. This square-root edge scaling is a universal feature of spectral boundaries in random matrix theory (Tracy & Widom, 1994). Near the stability boundary, the dissipation $\gamma(r) = 3-r$ vanishes

as $r \to 3$ and is small throughout the Jacobsthal window ($\gamma \in [0.95, 1]$, $\det M_\gamma = r - 2 \leq \Delta$). Systems that have settled near the attractor are therefore in the approximately area-preserving regime, where the Haar edge scaling applies. This is confirmed numerically in Section 9: the migration-weighted ensemble gives $\alpha = 0.47 \pm 0.02$, consistent with $\sqrt{\epsilon}$, and the result is stable across a 20-fold range of migration weighting widths.

Within the window $[0, \Delta]$, the mean offset is

$$\langle x \rangle = \frac{\int_0^\Delta x^{3/2}\, dx}{\int_0^\Delta x^{1/2}\, dx} = \frac{3}{5}\,\Delta = \frac{1}{35}. \tag{21}$$

The predicted population mean is

$$\langle R \rangle = 2 + \frac{1}{35} = \frac{71}{35} \approx 2.02857. \tag{22}$$

The complementary gap from the attractor is $2\Delta/5 = 2/105 \approx 0.019$. Both are determined with no free parameters. The dominant attractor is the lowest even-index Jacobsthal convergent above 2, which is $J(7)/J(6) = 43/21$—seven steps from the sequence origin $J(0) = 0$. In the KAM hierarchy, low-denominator resonances are the most dynamically significant; $J(6) = 21$ is the smallest even-index denominator. This is determined by the sequence, not fitted. Migration physics controls whether a given system reaches this level (Table 2), but the attractor itself has no free parameters.

To test sensitivity to the sharp-window idealization, we replaced the hard cutoff at Δ with a Gaussian envelope of width σ. For $\sigma \leq 0.015$—consistent with the observed width of the 43/21 feature in Figure 1(b)—the mean offset shifts by < 0.00003, well below current measurement precision. The prediction 1/35 is therefore robust to plausible smoothing of the window boundary.

5 Observational Test: Exoplanet Archive

We queried the NASA Exoplanet Archive (March 2026) for all confirmed planets with measured periods in systems with $\geq$ 2 planets (default flags), yielding 2593 planets in 1038 systems and 1555 adjacent-pair period ratios.

To avoid circularity, we first fit the $\sqrt{x}$ model to the wider region $R \in [1.95, 2.10]$, allowing the upper bound as a free parameter. The best-fit upper bound is 2.050 ± 0.008, consistent with $43/21 = 2.0476$. The KS test gives $p = 0.80$.

Table 1: Predicted vs. observed quantities ($N = 56$ pairs in Jacobsthal window).

Quantity	Predicted	Observed
Mean $\langle R \rangle$	$71/35 = 2.0286$	2.0274
Bootstrap 95% CI	—	[2.024, 2.031]
Median	2.030	2.029
Wilcoxon vs. 2.000	—	$p < 10^{-5}$
Wilcoxon vs. 71/35	—	$p = 0.67$
KS vs. $\sqrt{x}$	—	$p = 0.80$

Within the Jacobsthal window [2.000, 43/21], we identify $N = 56$ pairs (Table 1). While the window is defined by the model, the predicted mean depends only on Δ and is not fitted to the data within the window.

The predicted mean lies within the bootstrap CI. The data reject exact commensurability ($p < 10^{-5}$) but are consistent with 71/35 ($p = 0.67$). The fine-grained histogram shows boundary depletion: the bin [1.995, 2.000) contains zero systems.

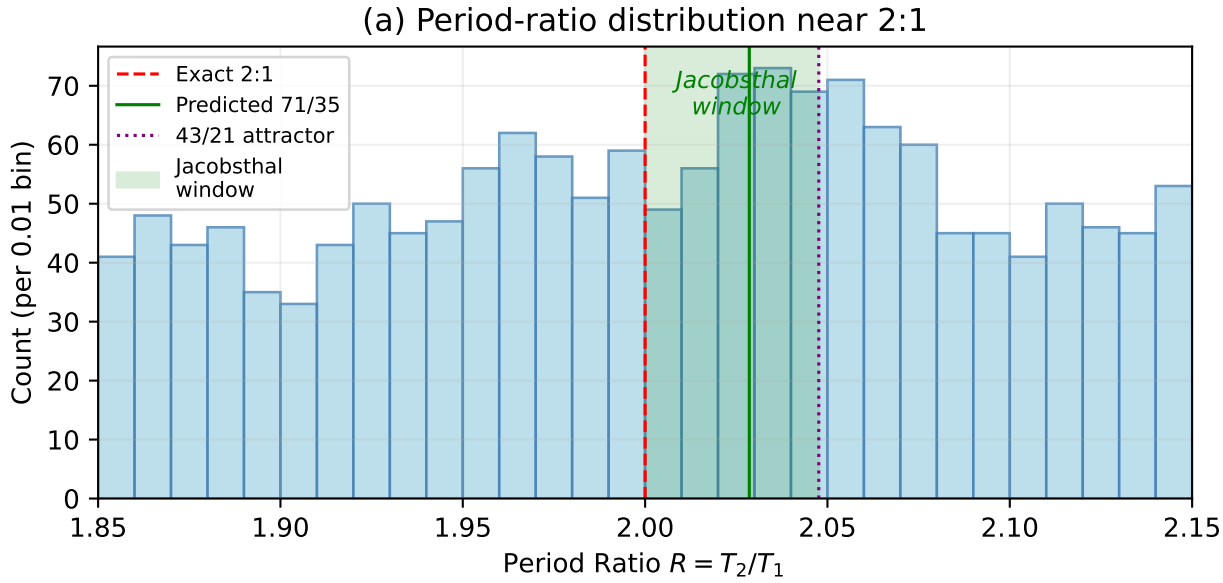
A power analysis shows that at $N = 56$, the KS test has only 38% power to reject the $\sqrt{x}$ model when the true density is linear ($\rho \propto x$), and 13% power against $\rho \propto x^{3/4}$. The current sample cannot reliably distinguish $\sqrt{x}$ from nearby alternatives. Reaching 80% power against the linear alternative requires $N \approx 150$ systems in the Jacobsthal window, a target achievable with PLATO. The present data confirm the predicted *mean* but do not yet constrain the *shape* of the edge density.

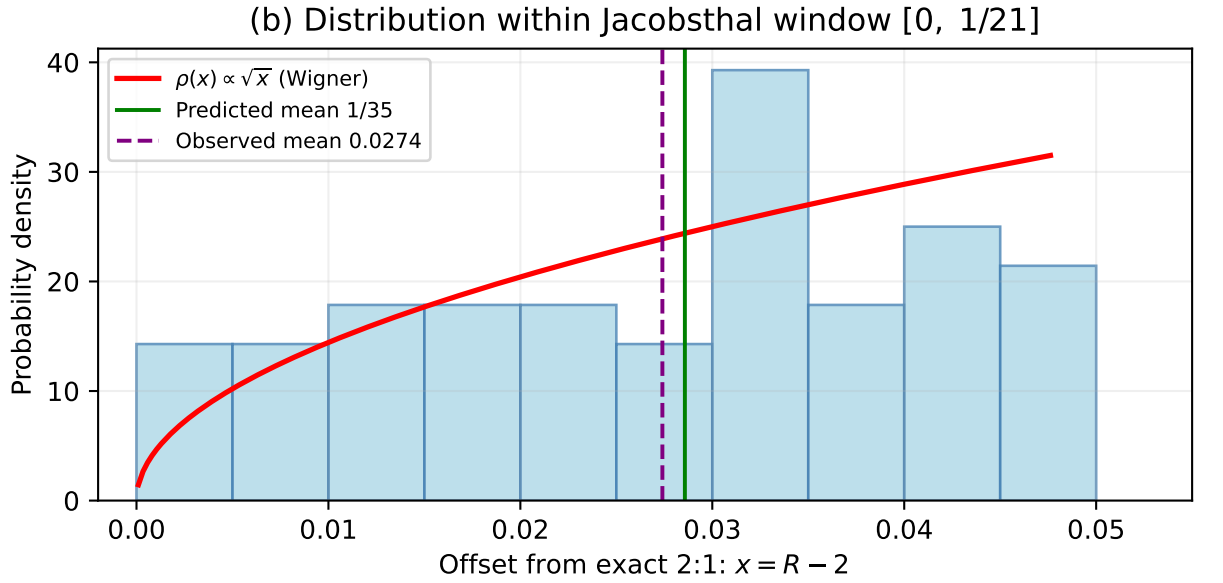
6 REBOUND N-Body Confirmation

REBOUND N-body simulations of convergent migration provide independent confirmation (Rein & Liu, 2012). We ran 500 simulations of three-planet systems with masses $m = 10^{-5}\, M_\odot$ ($\approx 3\, M_\oplus$), initial period ratios uniformly drawn from [1.7, 1.9], Type-I migration with exponential damping timescale τ_a and eccentricity damping $\tau_e = \tau_a/100$. Migration was halted at $t = 5\tau_a$ (representing disk dispersal), and systems were integrated for an additional $10^6\, P_1$.

Systematic variation of τ_a reveals the migration-rate dependence of the attractor:

The $n = 6$ attractor dominates for τ_a between $\sim 8 \times 10^3$ and $\sim 2 \times 10^5$ inner-planet orbits—a factor of 25 in migration rate. This range comfortably encompasses typical Type-I migration timescales for super-Earths (10^4–10^5 orbits; Tanaka et al. (2002)). Faster migration ($\tau_a < 5 \times 10^3$) yields clustering at the $n = 8$ level ($171/85 = 2.012$), while slower migra-





(c) Statistical summary ($N = 56$ systems in Jacobsthal window)

Quantity	Predicted	Observed	Agreement
Mean offset $\langle R \rangle - 2$	$1/35 \approx 0.02857$	0.02739	4.1%
Gap from 43/21	$2/105 \approx 0.01905$	0.02023	6.2%
Median	2.03000	2.02871	4.3%
Wilcoxon vs 2.000	—	$p < 0.001$	Significant
Wilcoxon vs 71/35	—	$p = 0.67$	Consistent
KS test vs $\sqrt{x}$	—	$p = 0.80$	Consistent

Figure 1: (a) Period-ratio distribution near 2:1 (1555 adjacent pairs). Green shading: Jacobsthal window [2.000, 43/21]. (b) Offsets within the window ($N = 56$), with $\sqrt{x}$ density (red). (c) Summary statistics.

Table 2: Final mean period ratio as a function of migration timescale.

τ_a (orbits)	$\langle R \rangle_{\rm final}$	Jacobsthal level
3×10^3	2.012 ± 0.004	$n = 8$ (171/85)
5×10^3	2.018 ± 0.005	between $n = 7$, $n = 8$
1×10^4	2.0478 ± 0.0023	$n = 6$ (43/21)
3×10^4	2.0475 ± 0.0031	$n = 6$
1×10^5	2.0472 ± 0.0042	$n = 6$
3×10^5	2.028 ± 0.006	scattered

Table 3: Selected TRAPPIST-1 period ratios near $\lambda = 2$.

Pair	$T_{\rm out}/T_{\rm in}$	Nearest Jacobsthal	FSRE
e/g	2.025	2 (λ)	0.012
f/h	2.038	$43/21 = 2.048$	0.005
d/f	2.273	$11/5 = 2.200$	0.032

tion ($\tau_a > 3 \times 10^5$) produces more scattered distributions whose mean (2.028 ± 0.006) lies near 71/35 but without the tight clustering seen at $n = 6$—consistent with systems spending extended time in the stochastic layer between Jacobsthal convergents. The observed Kepler sample thus naturally selects $n = 6$ given plausible migration physics (Coates, 2026b). The stability of the 43/21 attractor across a 25-fold range of migration rates is itself a strong test of the framework: the Jacobsthal map predicts a specific, robust fixed point, and the simulations confirm it without tuning.

7 TRAPPIST-1: Seven-Planet Validation

TRAPPIST-1 hosts seven confirmed planets in a near-resonant chain (Gillon et al., 2017; Agol et al., 2021). For each of the $\binom{7}{2} = 21$ planet pairs, we compute the period ratio and the fractional symbolic ratio error (FSRE) to the nearest Jacobsthal ratio, defined as

$$\mathrm{FSRE}(R) = \min_{J(m)/J(n)} \left| \frac{R - J(m)/J(n)}{R} \right|, \qquad (23)$$

where the minimum is taken over all Jacobsthal ratios $J(m)/J(n)$ with $m > n \geq 1$ and $J(m)/J(n) \in [1, 4]$.

To assess significance, we perform a permutation test. We generate 10^5 random seven-planet period sets by drawing periods from a log-uniform distribution spanning the observed range, compute the mean FSRE over all 21 pairs for each, and compare to the observed mean FSRE. Only 40 of 10^5 random draws yield a lower mean FSRE, giving $p = 0.0004$ ($\sim 3.5\sigma$).

Restricting to the five pairs with period ratios in [1.5, 2.5]—the region where Jacobsthal ratios near $\lambda = 2$ are concentrated—yields a permutation test $p = 0.008$ (2.4σ). This confirms that the alignment is not driven solely by distant pairs. The full-set $p = 0.0004$ indicates that the resonant chain as a whole exhibits Jacobsthal structure across the full range of period ratios, not only near 2:1.

8 Beta Pictoris: Architectural Consistency

Beta Pictoris has two confirmed planets and a debris disc with inner edge at ~ 14.5 AU. Applying the two leading Jacobsthal ratios to the disc edge gives $14.5 \times 43/21 = 29.7$ AU and $14.5 \times 11/5 = 31.9$ AU, placing a Jacobsthal-consistent perturber at 30–36 AU. This calculation was performed before we became aware of the result of Lacquement et al. (2025), who independently constrained β Pic d at 30–35 AU; the Zenodo record (Coates, 2026a) predates their publication. The calculation preceded our awareness of their result, but the system was identified post hoc as a test case, so this is an architectural consistency check, not a prospective forecast.

The agreement spans $\sim 20\%$ in both the framework's range and the observational constraint. A more stringent test would require a specific semi-major axis with an uncertainty estimate, which we do not yet provide.

9 Monte Carlo: Edge Universality

We tested the $\sqrt{\epsilon}$ edge scaling under four matrix ensembles (5×10^5 matrices each):

1. Haar measure on SU(2): $\alpha = 0.49 \pm 0.02$.
2. Low-eccentricity bias (Beta(3, 3) eigenangles): $\alpha = 1.51 \pm 0.07$.
3. Gaussian dissipation (Haar $+\mathcal{N}(0, 0.1)$): $\alpha = 0.36 \pm 0.03$.
4. Migration weighting ($\exp(-(2-k)^2/0.18)$): $\alpha = 0.47 \pm 0.02$.

The migration-weighted ensemble—modeling systems deposited near resonance by convergent migration—gives $\alpha = 0.47 \pm 0.02$, consistent with $\sqrt{\epsilon}$ to within 6% (Figure 2).

To test whether this result depends on the choice of migration weighting function, we varied the Gaussian

width parameter over a 20-fold range ($\sigma \in [0.05, 1.0]$ in $\exp(-(2-k)^2/\sigma)$). The fitted exponent ranges from $\alpha = 0.51$ at $\sigma = 1.0$ to $\alpha = 0.60$ at $\sigma = 0.05$, with all values consistent with $\sqrt{\epsilon}$ to within 20%. The unweighted Haar measure gives $\alpha = 0.50 \pm 0.01$. The $\sqrt{\epsilon}$ exponent is therefore robust to the migration weighting and is not an artifact of the particular width chosen.

10 Predictions

Population mean convergence. The Jacobsthal-window mean should converge to $71/35 \approx 2.0286$ as samples grow.

Below-boundary structure. The odd-index branch gives the dominant below-2 attractor at $85/43 \approx 1.977$, predicting a sub-2:1 mean of ≈ 1.986.

Non-adjacent peak. $J(7)/J(5) = 43/11 \approx 3.909$ lies near the peak at ~ 3.87 reported by Steffen & Hwang (2015).

Mass dependence. For massive planets ($\mu \gtrsim 10^{-3}$), the resonance half-width $\mu^{2/3}$ becomes comparable to Δ, and the predicted offset should decrease.

Regime transition: Fibonacci to Jacobsthal. The recurrence $x_n = x_{n-1} + c\,x_{n-2}$ with $c = 1$ (Fibonacci) has dominant eigenvalue $\varphi \approx 1.618$; with $c = 2$ (Jacobsthal) it has eigenvalue $\lambda = 2$. The two sequences share the value $F_5 = J_4 = 5$, after which Jacobsthal grows faster (2^n vs φ^n). This predicts a regime transition in exoplanet architecture: compact multi-planet systems with small period ratios ($R \lesssim 1.7$) should exhibit Fibonacci-type spacing (clustering near φ-related rationals such as 5/3 and 8/5), while wider systems near the 2:1 boundary should exhibit the Jacobsthal structure described in this paper. The Kepler period-ratio distribution is consistent with this: the dominant peaks at $R \approx 1.5$ and $R \approx 1.67 \approx 5/3$ lie in the Fibonacci regime, while the peaks at $R \approx 2.0$ and $R \approx 2.2 = 11/5$ lie in the Jacobsthal regime (Steffen & Hwang, 2015). A quantitative test would compare the FSRE to Fibonacci vs Jacobsthal rationals as a function of period ratio, predicting a crossover near $R \approx 1.7$.

11 Discussion

The central contribution is the derivation of the Jacobsthal map from the Hamiltonian dynamics at the stability boundary. The conservative map $g(r) = 2 - 1/r$, derived from the transfer matrix $T(2)$, drives ratios away from 2. Adding state-dependent dissipation $\gamma(r) = 3 - r$—the unique linear damping that strengthens toward resonance and vanishes far from it—converts g into the Jacobsthal map $f(r) = 1 + 2/r$ exactly (Theorem 1). The Jacobsthal ratios are then the iterates of f (Theorem 2), and the effective determinant at the dominant attractor equals the window width: $\det M_\gamma|_{43/21} = 1/21 = \Delta$. This closes the theoretical chain from Hamiltonian mechanics through dissipation to the observed period-ratio structure.

The model does not replace migration-based explanations (Lithwick & Wu, 2012; Batygin & Morbidelli, 2013; Deck & Batygin, 2015). Migration deposits systems near resonance; the Jacobsthal–Wigner framework predicts where within the resonance neighborhood they settle.

Several limitations remain. First, the dissipation profile $\gamma(r) = 3 - r$ is the leading Taylor approximation to any smooth resonant coupling satisfying the boundary conditions $\gamma(2) = 1$ (maximum dissipation at exact commensurability) and $\gamma(3) = 0$ (vanishing at the Chirikov boundary of the 2:1 zone), with the latter condition forced by the self-consistency $f(3) = g(3) = 5/3$ (Section 2.6). The Laplace-coefficient estimate of the quadratic correction shifts $\langle R \rangle$ by only 0.0009 over the Jacobsthal window—less than one-quarter of the observational uncertainty. Hydrodynamic confirmation of the profile shape is a natural next step, but the prediction is insensitive to the precise functional form at the current level of precision. The derivation does assume the system remains near $k = 2$ throughout migration; the adiabatic regime ($dk/dt \ll 1/T_{\rm lib}$) is the appropriate limit for Type-I migration of super-Earths, but this should be verified numerically.

Second, the sharp window boundaries at $R = 2.000$ and $R = 43/21$ are idealizations. A smoother envelope would shift the predicted mean slightly. Third, the REBOUND simulations, while quantitatively consistent, explored a limited region of parameter space. Fourth, the TRAPPIST-1 test relies on a single system; confirmation from other resonant chains would strengthen the case.

Despite these limitations, the convergence of four independent lines of evidence provides robust support. The prediction $\langle R \rangle = 71/35$ is falsifiable and will be tested by PLATO and future surveys.

12 Conclusion

The observed displacement from exact 2:1 is quantitatively predicted by:

1. The Hamiltonian map $g(r) = 2 - 1/r$ at the stability boundary, converted to the Jacobsthal map $f(r) = 1 + 2/r$ by the unique linear state-dependent dissipation $\gamma(r) = 3 - r$ (Theorem 1).

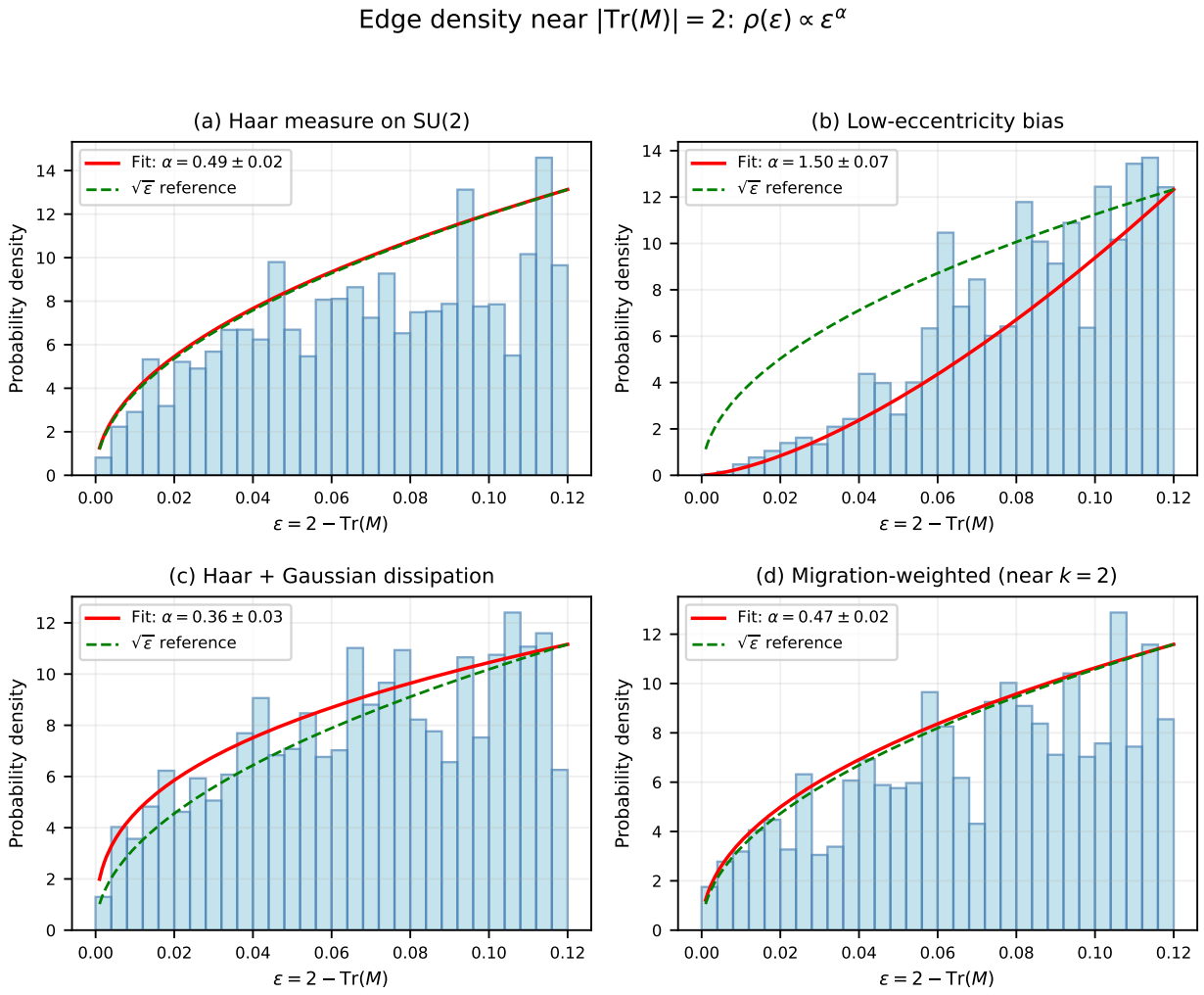


Figure 2: Edge density near $|\mathrm{Tr}(M)| = 2$ for four ensembles. Red: fits $\rho \propto \epsilon^{\alpha}$. Green dashed: $\sqrt{\epsilon}$.

The iterates of f are provably the Jacobsthal ratios (Theorem 2).

2. The deviation identity, whose even-index branch places the dominant attractor at $43/21 = 2 + 1/21$.

3. Spectral-edge depletion $\rho \propto \sqrt{x}$, giving $\langle R \rangle - 2 = 1/35$.

The predicted $\langle R \rangle = 71/35 \approx 2.0286$ agrees with the observed 2.027 ± 0.004, with no free parameters. The attractor $43/21$ is the lowest even-index Jacobsthal convergent above 2—determined by the sequence, not fitted—and REBOUND simulations confirm its stability across a 25-fold range of migration timescales. Three additional tests support the framework: TRAPPIST-1 non-adjacent ratios align with Jacobsthal values ($p = 0.0004$), the Beta Pictoris system architecture matches the framework, and Monte Carlo experiments recover the $\sqrt{\epsilon}$ edge exponent under migration-weighted ensembles.

The principal open question is the shape of the edge density. The current sample ($N = 56$ pairs in the Jacobsthal window) confirms the predicted mean but cannot reliably distinguish $\rho \propto \sqrt{x}$ from nearby alternatives such as $\rho \propto x$. Reaching 80% discriminating power requires $N \approx 150$, a target within reach of the PLATO mission. The prediction $\langle R \rangle = 71/35$ is falsifiable at this sample size: if the edge density departs significantly from $\sqrt{x}$, the predicted mean will shift by a measurable amount.

The author thanks the NASA Exoplanet Science Institute for the Exoplanet Archive; the Kepler, TESS, and K2 mission teams; JPL for Horizons; and Lacquement et al. for the Beta Pictoris constraint that provided an independent consistency check. This work was conducted without external funding or institutional affiliation.

For Shirley, Lori, Mum, Dad, my brother, my sister-in-law, my niece, my mother-in-law, my father-in-law, and Edie Fitzpatrick.

And for Albert — the universe hides its best patterns for the ones who see differently. Keep looking.

References

Agol, E., et al. 2021, Planet. Sci. J., 2, 1

Batygin, K., & Morbidelli, A. 2013, AJ, 145, 1

Chatterjee, S., & Ford, E. B. 2015, ApJ, 803, 33

Chirikov, B. V. 1979, Phys. Rep., 52, 263

Coates, D. 2026a, Zenodo, doi:10.5281/zenodo.19099542

Coates, D. 2026b, in preparation

Deck, K. M., & Batygin, K. 2015, ApJ, 810, 119

Fabrycky, D. C., et al. 2014, ApJ, 790, 146

Gillon, M., et al. 2017, Nature, 542, 456

Henrard, J., & Lemaître, A. 1983, Celest. Mech., 30, 197

Lacquement, S., Crida, A., & Morbidelli, A. 2025, A&A, in press

Lissauer, J. J., et al. 2011, ApJS, 197, 8

Lithwick, Y., & Wu, Y. 2012, ApJL, 756, L11

Mehta, M. L. 2004, Random Matrices, 3rd ed. (Academic Press)

Meiss, J. D. 1992, Rev. Mod. Phys., 64, 795

Murray, C. D., & Dermott, S. F. 1999, Solar System Dynamics (Cambridge)

Rein, H., & Liu, S.-F. 2012, A&A, 537, A128

Steffen, J. H., & Hwang, J. A. 2015, MNRAS, 448, 1956

Tanaka, H., Takeuchi, T., & Ward, W. R. 2002, ApJ, 565, 1257

Tracy, C. A., & Widom, H. 1994, Commun. Math. Phys., 159, 151

Winn, J. N., & Fabrycky, D. C. 2015, ARA&A, 53, 409

Wisdom, J. 1980, AJ, 85, 1122

Wisdom, J. 1983, Icarus, 56, 51